

Strain-Rate and Temperature Dependences of Deformation Behavior of AZ61Mg Alloy Processed by Multi-directional Forging Under Decreasing Temperature Conditions

メタデータ	言語: eng 出版者: 公開日: 2017-12-22 キーワード (Ja): キーワード (En): 作成者: メールアドレス: 所属:
URL	https://doi.org/10.24517/00049524

This work is licensed under a Creative Commons Attribution 3.0 International License.



Strain-rate and temperature dependences of deformation behavior of AZ61Mg alloy
processed by multi-directional forging under decreasing temperature conditions

C. WATANABE*†, R. MONZEN*, R. UEJI** and H. MIURA***

*Faculty of Mechanical Engineering, Kanazawa University (Kakuma-machi, Kanazawa 920-1192, Ishikawa, Japan).

**National Institute for Materials Science (1-2-1 Sengen, Tsukuba 305-0047, Ibaraki, Japan)

***Department of Mechanical Engineering, Toyohashi University of Technology (Tempaku-cho, Toyohashi 441-8580, Aichi, Japan)

†Author for correspondence: chihiro@se.kanazawa-u.ac.jp

ABSTRACT

Strain-rate and temperature dependences of deformation behavior of ultrafine-grained (UFGed) AZ61Mg alloy were examined. For this purpose, AZ61Mg alloy specimens were subjected to multi-directional forging (MDFing) under decreasing temperature conditions to have various grain sizes. The average grain sizes attained by MDFing to 1, 3, 6 and 9 passes were approximately 8, 2, 0.5 and 0.3 μm , respectively. A superior balance of the mechanical properties of strength and ductility at room temperature was achieved by MDFing to 3 passes and over. The strain-rate sensitivity of mechanical properties of the MDFed specimens increased with decreasing grain size. The specimens with grain sizes of 0.5 and 0.3 μm (0.5- or 0.3-specimen) exhibited stronger strain-rate and temperature dependences of total elongation than those with grain sizes of 8 and 2 μm (8- or 2-specimen). This can be partially ascribed to grain-boundary sliding, since an AFM observation revealed the occurrence of room-temperature grain-boundary sliding in the 0.3-specimen. The activation volume V^* for the 8-, 2- and 0.5-specimen increased with increasing temperature, while the 0.3-specimen exhibited an inverse temperature dependence of V^* . This suggests a change in deformation mechanism with decreasing grain size as well as the occurrence of grain-boundary sliding.

KEYWORDS: AZ61Mg alloy, multi-directional forging (MDF), ultrafine grain, deformation behavior, strain-rate sensitivity, deformation temperature

I. INTRODUCTION

Magnesium (Mg) alloys have great potential as structural materials owing to their high specific strength. Mg alloys are the lightest metals for practical use. The practical applications of Mg alloys have been, however, limited because of their low actual strength, and poor ductility due to their hexagonal-close-packed crystal structure. Numerous numbers of studies are carried out to improve the mechanical properties of Mg alloys. One of the most promising approaches is to enhance their ductility and strength through grain refinement. To obtain ultrafine-grained (UFGed) structure (grain size in submicron range), various severe plastic deformation methods have been applied to Mg alloys [1-4].

Miura and his colleagues reported that UFGed AZ31Mg [5, 6], AZ61Mg [6, 7] and AZ91Mg [6] alloys produced by multi-directional forging (MDFing) exhibited extremely high strength with reasonable ductility even at ambient temperature. Strength-ductility balances of the UFGed AZ series Mg alloys fabricated by MDFing are comparable to those of precipitation-hardened 2000 series Al alloys. In spite of such attractive mechanical properties of the UFGed Mg alloys, their nature is not widely investigated yet.

Recently, several investigators found that the strain-rate dependence of flow stress of various FCC metals became stronger as grain size decreased [8-11]. If this is also the case for HCP Mg alloys, UFGed Mg alloys are really attractive as structural materials for transportation equipment because of their high-energy absorption in dynamic straining, together with their superior specific strength. In the present study, AZ61Mg alloy specimens with different grain sizes processed by MDFing under decreasing temperature conditions were tensile-tested under various strain rates from 10^{-5} to 10^3 s^{-1} at some temperatures in order to examine the strain-rate and temperature dependences of deformation behavior.

2. EXPERIMENTAL

Rods of a commercial hot-extruded AZ61Mg alloy were annealed at 773 K (500 °C) for 2 hours to have homogeneous microstructure and an average grain size of approximately 20 μm . The annealed rods were cut into rectangular pieces with a dimension of 31 x 21 x 14 mm^3 (aspect ratio of 2.22 : 1.49 : 1). The pieces were then processed by multi-directional forging (MDFing) under decreasing temperature conditions. The MDFing processing was conducted using an Amsler-type universal testing machine at an initial strain rate of 10^{-3} s^{-1} . The first forging axis was parallel to the hot extruded axis, and a pass strain of $\Delta\varepsilon = 0.8$ was employed. During the MDFing, forging temperature was gradually decreased pass by pass from 623 K (350 °C) to 423 K (150 °C). The MDFing processing was carried out up to a maximum cumulative strain of $\Sigma\Delta\varepsilon = 7.2$, i.e., total of nine passes. The principle and the practical detail of MDFing under decreasing temperature conditions are described elsewhere [5-7].

The multi-directional-forged (MDFed) specimens were cut into 3-mm disks parallel to the final forging axis and were mechanically ground down to 0.2 mm in thickness. Thin foils for transmission electron microscopy (TEM) observations were prepared using a twin-jet electro polishing method with a solution of 92 vol pct ethanol, 6 vol pct 2-butoxyethanol and 2 vol pct perchloric acid under a condition of 233 K (-40 °C) and 12.5 V. TEM observations were performed using a JEOL 2000EX and a 2010FEF microscope at an operating voltage of 200 kV.

Specimens for tensile tests with a gage dimension of 2.5 x 5 x 0.7 mm^3 were spark-cut from the MDFed specimens, so that the loading axis was perpendicular to the final forging axis. The flat tensile specimens were mirror-finished by mechanical polishing with SiC papers, with diamond suspensions of 3 through 0.1 μm and then with an active oxide suspensions bearing reagents. Tensile tests were performed on a sensing-block-type testing machine (Saginomiya HMH206) under an initial strain rate $\dot{\varepsilon}$ ranging from 10^{-5} to 10^3 s^{-1} at room temperature (RT). Quasi-static tensile tests at three different temperatures of 77 K (-196 °C), 200 K (-73 °C) and RT were also conducted on an Instron-type mechanical testing machine (Shimadzu Autograph AG-X) under $\dot{\varepsilon} = 10^{-3} \text{ s}^{-1}$.

Moreover, strain-rate jump tests were carried out between $\dot{\epsilon}_1 = 10^{-4}$ and $\dot{\epsilon}_2 = 10^{-3} \text{ s}^{-1}$ at 77 K (-196 °C), 200 K (-73 °C) and RT. The surface morphology of the specimens before and after tensile tests was investigated using optical microscopy and atomic force microscopy (AFM, JOEL JSTM-4200D).

III. RESULTS

A. Microstructure and tensile behavior

The grain sizes of the specimens prepared by MDFing decreased with increasing MDFing passes, i.e., with increasing cumulative strain $\Sigma\Delta\epsilon$. Figure 1 depicts a Bright-field TEM image of the specimen after MDFing to 9 passes. The inset is the corresponding selected-area diffraction pattern (SADP) taken using a selected-area aperture having a diameter of 2.5 μm . Nearly continuous diffraction rings that can be seen in the SADP shown in Figure 1 indicates that roughly equiaxed grains are separated by a reasonably high fraction of high-angle boundaries. The average grain sizes \bar{d} of the specimens after MDF processing to 1, 3, 6 and 9 passes, i.e. $\Sigma\Delta\epsilon = 0.8, 2.4, 4.8$ and 7.2 , were $8.3 \pm 1.2, 2.1 \pm 0.8, 0.5 \pm 0.1$ and $0.3 \pm 0.1 \mu\text{m}$, respectively. Approximately 100 separate measurements via the liner intercept method were performed to estimate \bar{d} of each specimen. It is obvious that the MDF processing resulted in significant grain refinement from an initial grain size of 20 μm . Hereafter the specimens with $\bar{d} = 8.3, 2.1, 0.5$ and 0.3 will be referred to as 8-, 2-, 0.5- and 0.3-specimens, respectively.

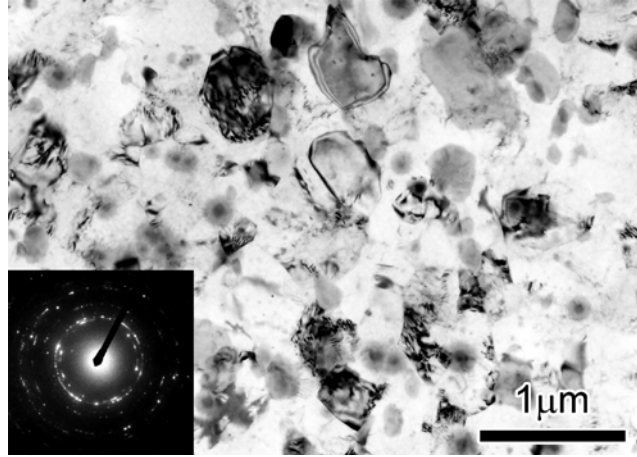


Fig. 1-Bright-field TEM micrograph of an AZ61Mg specimen processed by MDFing of 9 passes ($\Sigma\Delta\varepsilon = 7.2$). The inset is the corresponding selected-area diffraction pattern taken using a selected-area aperture of $2.5\ \mu\text{m}$ in diameter.

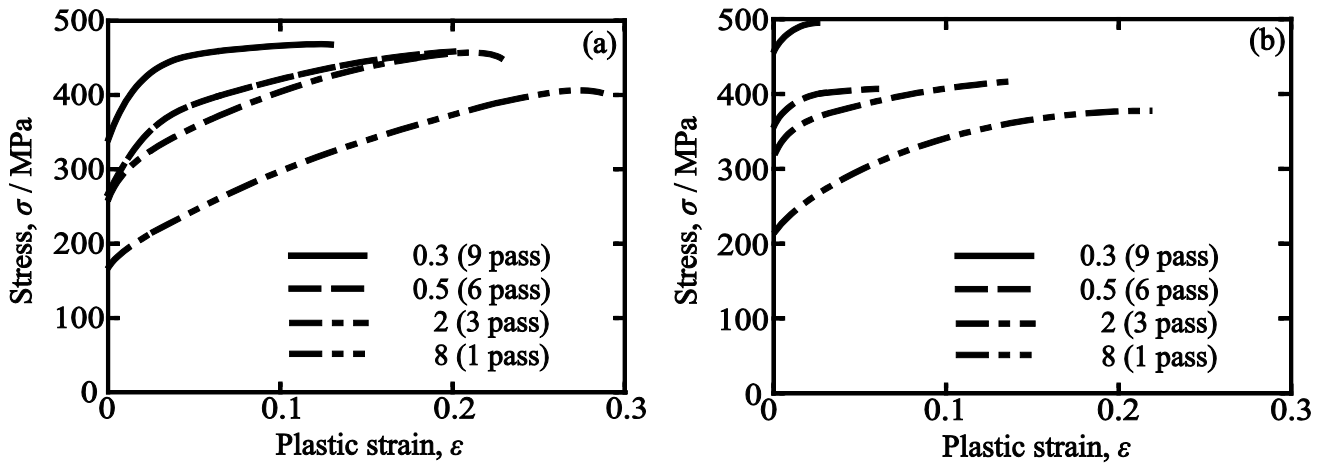


Fig. 2-Stress–strain curves of AZ61Mg specimens with different grain sizes produced by MDFing of different passes, tested under strain rates of (a) 10^{-3} and (b) $10^3\ \text{s}^{-1}$ at RT.

Figures 2(a) and (b) show typical nominal stress–strain curves of the MDFed specimens obtained by tensile tests at RT under $\dot{\varepsilon} = 10^{-3}$ and $10^3\ \text{s}^{-1}$. In either case of $\dot{\varepsilon} = 10^{-3}$ and $10^3\ \text{s}^{-1}$, the strength increases with decreasing grain size, while the fracture strain exhibits a reverse tendency. The strengths of the specimens tested under $\dot{\varepsilon} = 10^{-3}\ \text{s}^{-1}$ are lower than those tested under $\dot{\varepsilon} = 10^3\ \text{s}^{-1}$. Table 1 summarizes the ultimate tensile stress σ_{UTS} , 0.2 pct proof stress $\sigma_{0.2}$, and fracture strain ε_f of the specimens tested at RT under $\dot{\varepsilon} = 10^{-3}\ \text{s}^{-1}$. The previous reported data for ZK60A-T5 [12] and A6061-T651 [13] alloys tested under $\dot{\varepsilon} = 10^{-3}\ \text{s}^{-1}$ and $\dot{\varepsilon} = 6 \times 10^2\ \text{s}^{-1}$ respectively are also listed in

Table 1 for the sake of comparison. The ZK60A Mg alloy is a conventional wrought Mg alloy used for application of high strength parts for transportation equipment, such as gear boxes, rotor hubs, bicycle frames and road wheels. The A6061 Al alloy is a typical competitive one. It should be noted in Table 1 that the 2-, 0.5- and 0.3-specimens possess evidently higher proof stresses and tensile strengths than the ZK60A Mg and A6061 Al alloys. Absorbed energies W till fracture for the MD Fed specimens deformed at RT under a dynamic straining condition of $\dot{\epsilon} = 10^3 \text{ s}^{-1}$ were estimated from integration of data in the measured stress-strain curves in Figure 2(b), and are listed in Table 2, together with ϵ_f and specific strength $\sigma_{\text{UTS}} / \rho$. Here, ρ ($= 1.74 \text{ Mg m}^{-3}$) is the specific density of Mg [14]. Although the specific strength increases with decreasing grain size, the absorbed energy shows a reverse tendency. The reported values of $\sigma_{\text{UTS}} / \rho$ for the ZK60A [12] and A6061 [13] alloys tested under $\dot{\epsilon} = 10^3 \text{ s}^{-1}$ and $\dot{\epsilon} = 6 \times 10^2 \text{ s}^{-1}$ respectively are also shown in Table 2. The 0.5- and 0.3-specimens possess larger specific strengths than the ZK60A and A6061 alloys. Moreover, the balances of the specific strength and absorbed energy for the 0.5- and 0.3-specimens are superior to that of the A6061 alloy, and are comparable to that of the ZK60A alloy.

Figure 3 presents the dependence of fracture strain ϵ_f at RT on the applied strain rate $\dot{\epsilon}$ for the 8-, 2-, 0.5- and 0.3-specimens. The fracture strain of the 0.5- and 0.3-specimens depends notably on the strain rate $\dot{\epsilon}$. It rapidly decreases with increasing $\dot{\epsilon}$. The specimens also exhibit a strong temperature dependence of ϵ_f , as shown in Figure 4, where the fracture strains obtained by tensile tests at 77 K (-196 °C), 200 K (-73 °C) and RT under $\dot{\epsilon} = 10^{-3} \text{ s}^{-1}$ are presented as a function of grain size. At RT, the fracture strain gradually decreases with decreasing \bar{d} , whereas at 77 K (-196 °C) and 200 K (-73 °C), it exhibits a sharp drop below around 2 μm .

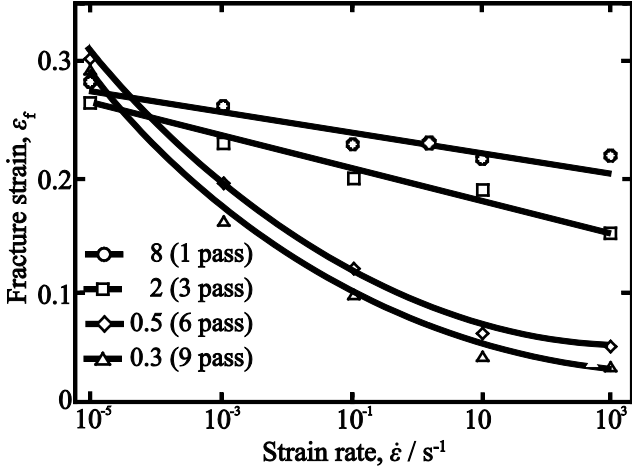


Fig. 3-Strain rate dependence of the fracture strain of AZ61Mg specimens with different grain sizes fabricated by MDFing. Tensile tests were performed at RT.

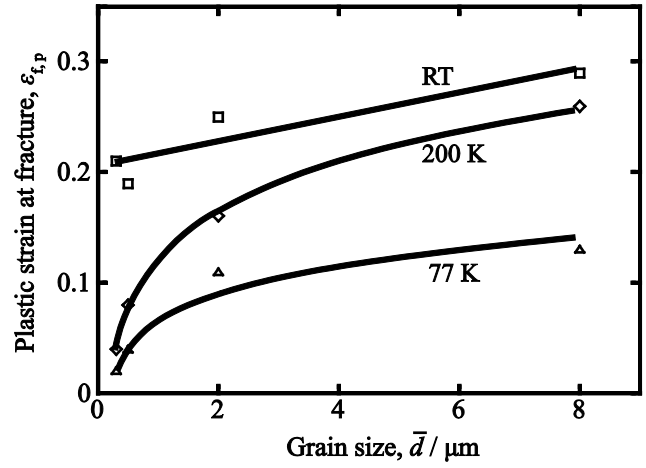


Fig. 4-Grain size dependence of the fracture strain of AZ61Mg specimens fabricated by MDFing under a constant strain rate of 10^{-3} s^{-1} at 77 K (-196 °C), 200 K (-73 °C) and RT.

B. Strain-rate sensitivity

Figure 5 shows the 0.2 pct proof stress at RT plotted as a function of the strain rate $\dot{\epsilon}$ on logarithmic scales for the 8-, 2-, 0.5- and 0.3-specimens. The 0.2 pct proof stresses of all of the specimens increase monotonically with increasing of $\dot{\epsilon}$. A linear relationship is observed between $\log \sigma_{0.2}$ and $\log \dot{\epsilon}$ for the 8- and 2-specimens tensile-tested between $\dot{\epsilon} = 10^{-5} \text{ s}^{-1}$ and 10^3 s^{-1} , and for the 0.5- and 0.3-specimens tensile-tested between $\dot{\epsilon} = 10^{-3} \text{ s}^{-1}$ and 10^3 s^{-1} . The strain-rate sensitivity m is calculated by the following equation.

$$m = \frac{\partial \ln \sigma}{\partial \ln \dot{\epsilon}} \quad (1)$$

The slopes of $\log \sigma_{0.2}$ versus $\log \dot{\epsilon}$ plot in Figure 5 yield values of m . Using the least-squares method, the values were obtained and are summarized in Table 3. For the 0.5- and 0.3-specimens, the m -values estimated under conditions of $\dot{\epsilon} \geq 10^{-3} \text{ s}^{-1}$ are listed in Table 3.

The slopes of the 0.5- and 0.3-specimens in Figure 5 can be roughly divided into two regions depending on strain rate, that is, either less or more than $\dot{\epsilon} = 10^{-3} \text{ s}^{-1}$. The m -values of about 0.04 and 0.06 for the 0.5- and 0.3-specimens in the case of $\dot{\epsilon} \leq 10^{-3}$ are larger than those (0.019 and 0.023) obtained at the condition of $\dot{\epsilon} \geq 10^{-3}$. Table 3 shows that the value of m increases as the

grain size decreases.

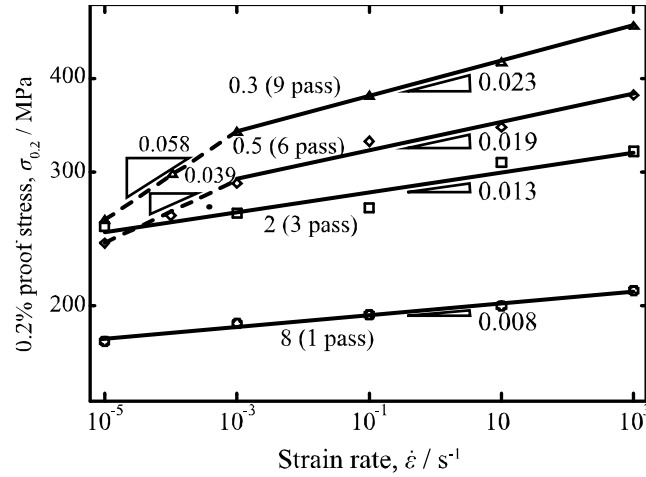


Fig. 5-Change in the 0.2 pct proof stress with strain rate for AZ61Mg specimens with different grain sizes. Tensile tests were performed at RT.

Strain-rate jump tests were carried out on an Instron-type mechanical testing machine at 77 K (-196 °C), 200 K (-73 °C) and RT under strain rates of 10^{-4} and 10^{-3} s $^{-1}$. Stress-strain responses obtained are displayed in Figure 6. Strain-rate jump tests at 77 K (-196 °C) of the 0.3-specimen could not be performed between 10^{-4} and 10^{-3} s $^{-1}$, since the specimen exhibited only a few percent of plastic elongation at 77 K (-196 °C) (see Figures 4 and 6(a)). The change in the flow stress $\Delta\sigma$ associated with the sudden strain-rate jump and down tends to become more evident with decreasing grain size. The strain-rate sensitivity m can be also obtained from strain-rate jump tests. When a strain-rate jump from $\dot{\epsilon}_1$ to $\dot{\epsilon}_2$ causes a change in the flow stress from σ_1 to σ_2 , m is given by

$$m \approx \frac{\Delta\sigma}{\sigma\Delta\ln\dot{\epsilon}} \approx \frac{(\sigma_2 - \sigma_1)}{\left[\frac{\sigma_2 - \sigma_1}{2}\right] \ln\left(\frac{\dot{\epsilon}_2}{\dot{\epsilon}_1}\right)}. \quad (2)$$

The average values of m obtained from strain-rate jump tests at RT are summarized in Table 3. These estimated m -values from strain-jump tests are in reasonable agreement with those obtained from tensile tests. The temperature dependence of strain-rate sensitivity m for the 8-, 2-, 0.5, and 0.3-specimens was plotted in Figure 7, where m values were obtained at identical plastic strain of 5

pct. It is evident that the m value decreases with decreasing T for all of the specimens. What is more interesting in Figure 7 is that, the m value at RT increases with decreasing the grain size, whereas the m values at 77 K (-196 °C) are almost the same, independent of the grain size.

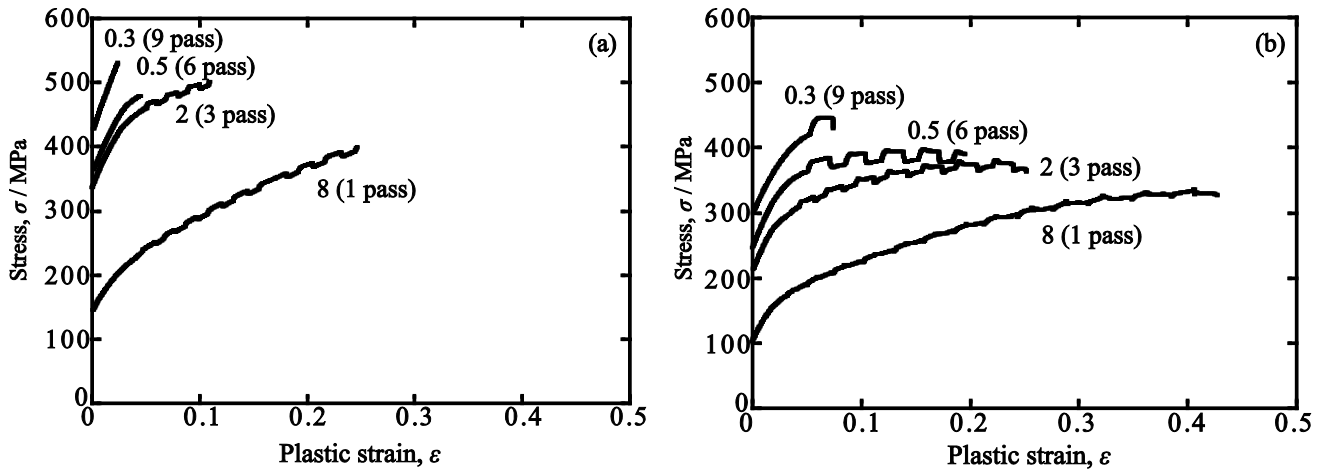


Fig. 6-Stress-strain curves of AZ61Mg specimens with different grain sizes at (a) 77 K (-196 °C) and (b) RT. The steps on the curves are changes in the flow stress caused by strain-rate jump tests between 10^{-4} and 10^{-3} s $^{-1}$.

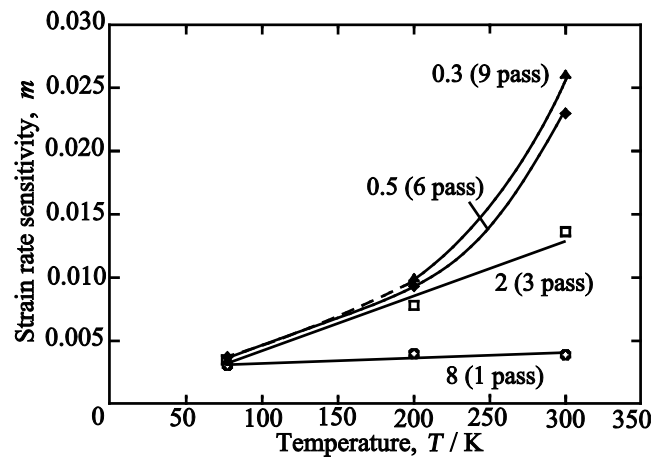


Fig. 7-Relationship between the strain rate sensitivity m and deformation temperature T for AZ61Mg specimens with different grain sizes processed by MDFing.

C. Surface morphology

The surface morphology during tensile test was observed by means of AFM. Figures 8(a) and (b) show representative AFM images of the 0.3-specimen before and after tensile deformation to plastic strain of 5 pct at RT under $\dot{\epsilon} = 10^{-5}$ s $^{-1}$. Before the deformation, slight surface relief

corresponding to the component UFGs is visible in Figure 8(a). After the tensile deformation, however, offsets or displacements among the adjacent grains made their individual outlines more distinct (Figure 8 (b)). Figures 9(a), (b) and (c) present AFM images taken from the same area of the 0.3-specimen before tensile deformation and after tensile deformation to 5 and 15 pct strains at RT under $\dot{\epsilon} = 10^{-5} \text{ s}^{-1}$. Most grain boundaries became visible more clearly with increasing plastic strain. In addition, the amounts of offset among the adjacent grains also increased at larger plastic strain, as displayed in height profiles in Figure 9. The arithmetic average roughness R_{ave} was calculated from the height profiles along the horizontal lines in Figure 9. These R_{ave} -values as a function of plastic strain are plotted in Figure 10. It is obvious that the R_{ave} becomes larger with increasing strain. For the sake of comparison, AFM observations of the 0.3-specimens deformed to 10 pct under $\dot{\epsilon} = 10^{-1} \text{ s}^{-1}$ at RT and to 5 pct under $\dot{\epsilon} = 10^{-5} \text{ s}^{-1}$ at 200 K (-73 °C) were also carried out. The measured values of R_{ave} were about 3.3 and 3.5 nm respectively. These values are obviously smaller than that of the specimen deformed to 5 pct under $\dot{\epsilon} = 10^{-5} \text{ s}^{-1}$ at RT or almost comparable with that before deformation. Thus the amount of offsets at grain boundaries during plastic deformation sensitively depends on strain rate and temperature.

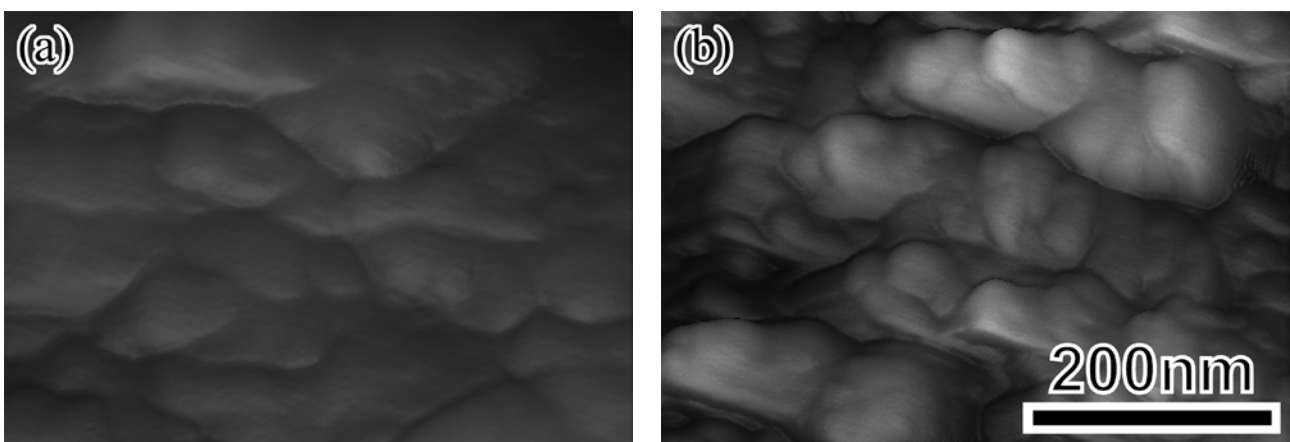


Fig. 8-AFM images of an AZ61Mg specimen with a grain size of 0.3 μm (a) before and (b) after tensile deformation of 5 pct plastic strain at RT under a strain-rate of 10^{-5} s^{-1} .

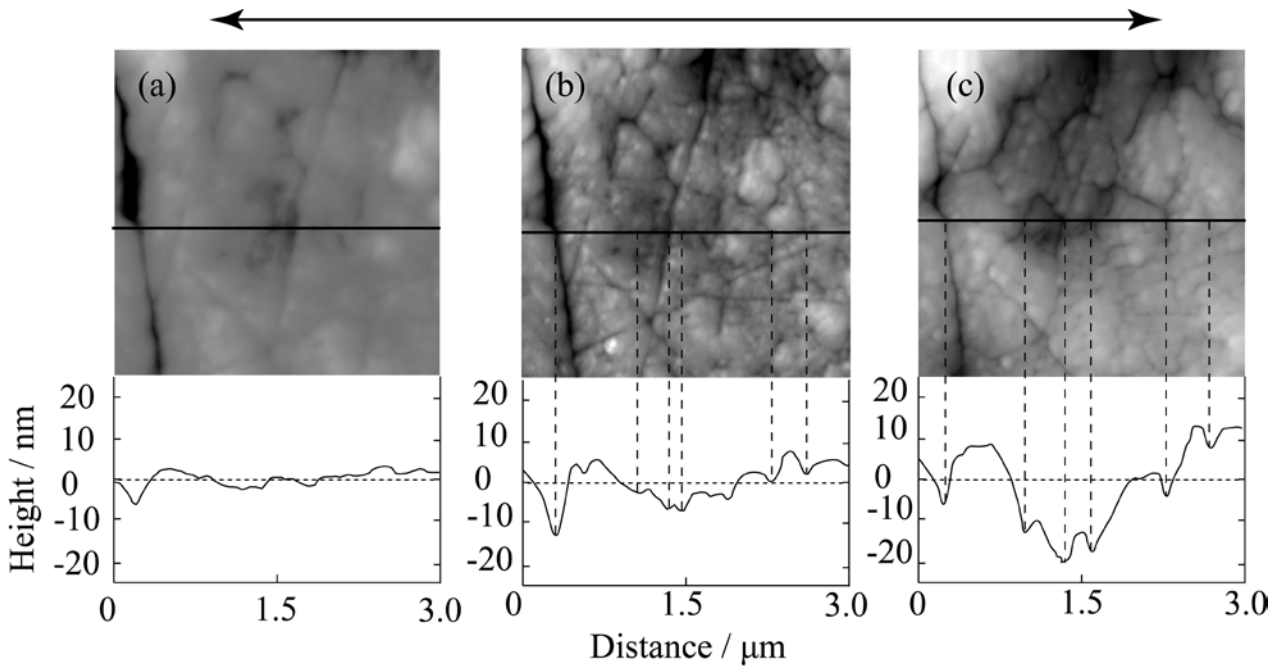


Fig. 9-AFM images and their sectional height profiles of an AZ61Mg specimen with a grain size of $0.3 \mu\text{m}$ (a) before and after tensile deformation of (b) 5 pct and (c) 15 pct plastic strain at RT under a strain-rate of 10^{-5} s^{-1} . All the images were taken from the same area. The arrow indicates the tensile axis.

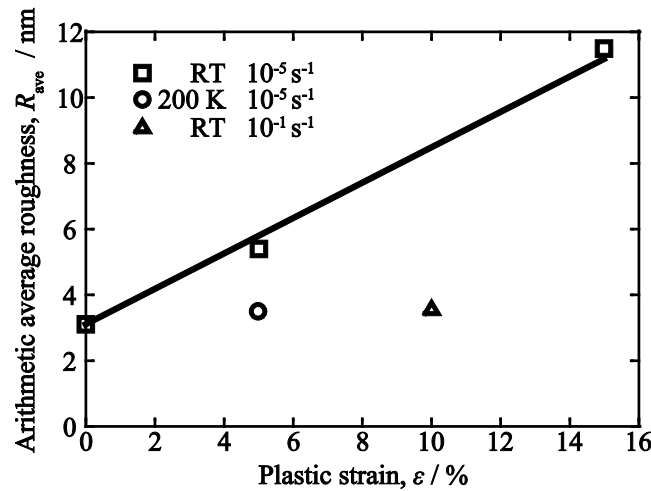


Fig. 10-Change in the arithmetic average roughness R_{ave} with applied plastic strain under several deformation conditions for an AZ61Mg specimen with a grain size of $0.3 \mu\text{m}$.

IV. DISCUSSION

In this study, the microstructure and deformation behavior of UFGed AZ61Mg specimens fabricated by MDF method were precisely investigated. Tensile strength of the MDFed specimens is raised with decreasing grain size, while ductility reduces (Table 1). The strength and fracture strain strongly depend on the strain rate and grain size (Figures 2-5). The strain-rate sensitivity m increases

with decreasing grain size (Table 3). However, the grain size dependence of m vanishes as temperature lowers (Figure 7). Similar dependency of m on the temperature and grain size of UFGed FCC metals has been reported already [15-17]. Although the m value itself is a phenomenological parameter obtained by mechanical testing, m is assumed to be related to thermally-activated plastic deformation process via activation volume V^* , as described by Kato *et al.* [18],

$$V^* = \frac{M_T kT}{m\sigma} \quad (3)$$

where M_T is the Taylor factor and kT has its usual meaning. From the results shown in Figure 7 and equation (3), the normalized V^* / b^3 values can be obtained. Figure 11 summarizes the temperature dependence of V^* / b^3 for the 8-, 2-, 0.5- and 0.3-specimens. Here, b ($= 0.3209$ nm [14]) is the magnitude of Burgers vector for basal slip system in Mg. The value of Taylor factor $M_T = 0.65$, when assumed that the basal slip system is a sole mechanism of plastic deformation [19], was used. In the 8-, 2- and 0.5-specimens, the value of V^* / b^3 increases with increasing T , whereas the 0.3-specimen exhibits a reversed tendency, that is, a decrease in V^* / b^3 value with increasing T . This is a suggestion that the deformation mechanism of the 0.3-specimen differs from that of the specimens with larger grain sizes. The former result is similar to those of single crystals and coarse-grained polycrystals of FCC metals [20, 21]. The latter result is also in qualitative agreement with the result that the activation volume for FCC metals with the grain sizes ranging from 10 nm to 1 μ m decreases with increasing T at temperatures below RT [22-24].

Recently, Kato *et al.* [18] have suggested de-pinning and glide mechanisms of dislocations in UFG metals without in-grain dislocation sources. Moreover, Kato has also pointed out that a thermally-activated dislocation de-pinning process can occur at one pinning point within a grain boundary after bowing out of dislocations from grain boundaries [25]. Kunimine *et al.* employed their model in order to explain the inverse temperature dependence of V^* in the UFGed Cu [26]. According to the model of Kato [25], the activation volume V^* is expressed as a function of effective stress τ^* as [26]

$$V^* \approx \frac{\tau^* w^* L^2}{2\mu} \left(1 + \frac{\tau^{*2} L^2}{2\mu^2 b^2} \right), \quad (4)$$

where μ is the shear modulus, w^* is the activation distance, and L is the distance between the pinning points on the grain boundary. The value of w^* is in the order of b [18]. The average of L is written as [18]

$$L = \frac{\bar{d} + 2\lambda}{3}. \quad (5)$$

Here, λ is the minimum distance between the pinning points on the grain boundary. The value of λ is approximately 10 nm [18, 25]. Since τ^* decreases with increasing T , equation (4) naturally indicates the decrease in V^* with increasing T . Therefore, the inverse temperature dependence of V^* observed in the 0.3-specimen (Figure 11) can be reasonably explained by the model of Kato.

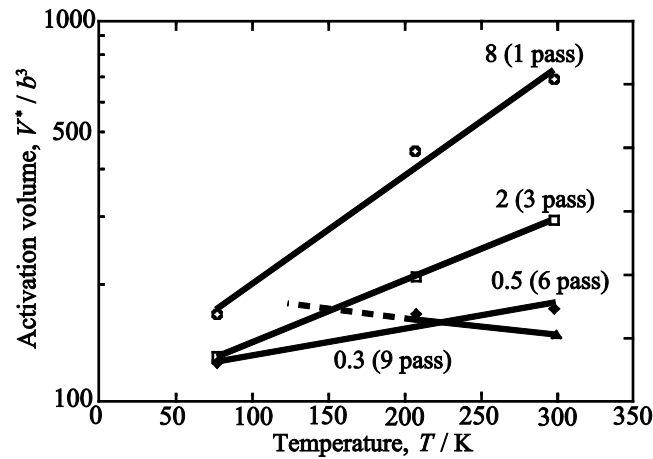


Fig. 11-Relationship between the normalized activation volume V^* / b^3 and deformation temperature T for AZ61Mg specimens with different grain sizes.

As shown in Figures 3 and 4, the strain-rate and temperature dependences of the fracture strain of the 0.5- and 0.3-specimens are much larger than those of the 8- and 2-specimens. Finally, this will be discussed.

Koike *et al.* [27] experimentally showed that grain-boundary sliding (GBS) took place even at RT during tensile deformation of AZ31Mg alloy with an average grain size of about 8 μm by

measuring the displacements of scribed lines across grain boundaries of deformed samples. The contribution of GBS to the total strain, that at RT was estimated to be approximately 8 pct, increased with increasing temperature. Although the occurrence of GBS in the 8- and 2- specimens at RT was examined by the same method as Koike *et al.* [27], the displacements of scribed lines across the grain boundaries of the specimens were not detected by scanning electron microscopy (SEM) observations.

Figure 12 depicts a bright-field TEM image of the 2-specimen. Many precipitates with sizes of 100 ~ 300 nm were mainly formed on boundaries, as indicated by arrows in Fig. 12. Analyses of SADPs taken from the boundary precipitates revealed that the precipitated phase was β -Mg₁₇Al₁₂. The existence of boundary β -precipitates were also confirmed in the 8-specimen. It seems that the β -precipitates were formed during MDFing or cooling down from MDFing temperature. It is well-known that the existence of boundary precipitates strongly inhibits GBS [28, 29, 30]. It can thus be said that the amount of GBS in the present alloy with the boundary β -precipitates were much smaller than that of the single-phase AZ31Mg alloy used by Koike *et al.* [27].

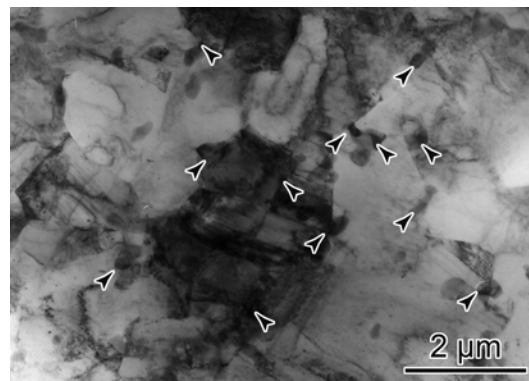


Fig. 12-Bright-field TEM micrograph of an AZ61Mg specimen processed by MDFing of 3 passes ($\Sigma\Delta\varepsilon = 2.4$). The arrows indicate β -Mg₁₇Al₁₂ precipitates.

On the other hand, Miura *et al.* reported that GBS can take place more extensively with decreasing the grain size of AZ61Mg alloy down to submicron order [31]. This result and the result

shown by Koike *et al.* [27] strongly suggest that GBS can occur even at RT in the 0.3-specimen of the present AZ61Mg alloy. However, the much smaller grain size of about 0.3 μm in the 0.3-specimen did not allow us to directly investigate GBS by SEM. On the other hand, offsets among the adjacent grains were found in the 0.3-specimens by the AFM observation after deformation (Figure 8), and their heights became larger with increasing strain (Figure 9). Moreover, the mean offset heights showed the strong dependences on the strain rate and temperature (Figure 10). Therefore, we conclude that the observed offsets were induced by GBS.

Recently, Miura *et al.* examined the superplasticity behavior of AZ61Mg alloy with an average grain size of 0.3 μm fabricated by MDFing under decreasing temperature conditions [31]. Superplasticity of 680 pct elongation to fracture was achieved at 423 K (150 °C) under a strain rate of 10^{-4} s^{-1} . The observed superplasticity of the UFGed Mg alloy was mainly attributed to "pure" GBS caused by grain-boundary diffusion. The values of the strain-rate sensitivity m obtained at RT in Table 3 are much smaller than that of 0.74 at 423 K (150 °C) reported by Miura *et al.* [31]. It can thus be said that the contribution of GBS toward total strain at lower temperatures must be considerably small. Koike *et al.* pointed out that GBS which occurred in AZ31Mg alloy below 373 K (100 °C) is categorized as "slip-induced" GBS related to inhomogeneous plastic deformation [27]. When GBS occurs, accommodation process is needed that includes the dislocation motion [32, 33], diffusional flow [34, 35] and so on. On the other hand, Monzen *et al.* measured grain-boundary viscosity in Cu, and showed that the viscosity intensely increased with decreasing temperature [36]. They also explained the temperature dependence of GBS using grain-boundary viscous sliding. The viscous sliding model of grain boundary predicts the extensive occurrence of GBS of the present UFGed Mg alloy at RT under a low strain-rate of 10^{-5} s^{-1} . However, GBS becomes rapidly difficult at lower temperatures or higher strain-rates due to intensively raised viscosity. Although actual accommodation process for the slip-induced GBS in Mg alloys has not been clarified yet, the strain rate and temperature dependences of mean offset heights in Figure 10 suggest that diffusional process is related to the slip-induced GBS. Therefore, the observed strong strain-rate and temperature

dependences of total elongation to fracture for the 0.5- and 0.3-specimens in Figures 3 and 4 can be partially attributed to the GBS.

V. CONCLUSIONS

The strain rate and temperature dependences of mechanical properties of AZ61Mg alloy specimens with various grain sizes were precisely and systematically investigated. The grain size was controlled by multi-directional forging (MDFing) under decreasing temperature conditions. Experimental and theoretical analyses of the strain rate and temperature dependences of the mechanical properties yielded the following conclusions.

- (1) MDFing of AZ61Mg alloy was successfully applied to obtain homogeneous microstructures. MDFing to 1, 3, 6 and 9 passes resulted in average grain sizes of 8, 2, 0.5 and 0.3 μm , respectively. A superior balance of mechanical properties of high strength and ductility at room temperature was achieved by the grain refinement.
- (2) The strain-rate sensitivity m became larger as grain size decreased. Furthermore, ultrafine-grained AZ61Mg specimens with average grain sizes of 0.5 and 0.3 μm exhibited strong strain-rate and temperature dependences of ductility.
- (3) The activation volume V^* estimated from values of m became larger with increasing temperature in the specimens with average grain sizes of 0.5 μm (0.5-specimen) and over. In contrast, the specimen with an average grain size of 0.3 μm (0.3-specimen) exhibited an inverse temperature dependence of V^* .
- (4) An AFM observation of the 0.3-specimen deformed in tension showed the occurrence of grain-boundary sliding. The strong strain-rate and temperature dependences of ductility of the 0.3-

and 0.5-specimen are partially attributed to the grain-boundary sliding.

ACKNOWLEDGEMENTS

This work was partially supported by a Grant-in-Aid for Scientific Research on Innovative Areas, "Bulk Nanostructured Metals", through MEXT, Japan, Contract No. 22102002. The authors would also like to acknowledge the financial support of Japan Science and Technology Agency (JST) under Industry-Academia Collaborative R&D Program "Heterogeneous Structure Control: Towards Innovative Development of Metallic Structural Materials".

REFERENCES

1. M. Kai, Z. Horita and T. G. Langdon: *Mater. Sci. Eng. A*, 2008, vol. 488, pp. 117-124.
2. R. Lapovok, P. F. Thomson and R. Cottam: *J. Mater. Sci.*, 2005, vol. 40, pp. 1699-1708.
3. A. Yamashita, Z. Horita and T. G. Langdon: *Mater. Sci. Eng. A*, 2001, vol. 300, pp. 142-147.
4. Y. Yoshida, L. Cisar, S. Camado and Y. Kojima: *J. JILM*, 2002, vol. 52, pp. 559-565.
5. J. Xing, X. Yang, H. Miura and T. Sakai: *Mater. Trans.*, 2008, vol. 49, pp. 69-75.
6. H. Miura, X. Yang and T. Sakai: *Rev. Adv. Mater. Sci.*, 2013, vol. 33, pp. 92-96.
7. H. Miura, G. Yu and X. Yang: *Mater. Sci. Eng. A*, 2011, vol. 528, pp. 6981-6992.
8. Y. M. Wang and E. Ma: *Appl. Phys. Lett.*, 2003, vol. 83, pp. 3165-3167.
9. Q. Wei, S. Cheng, K. T. Ramesh and E. Ma: *Mater. Sci. Eng. A*, 2004, vol. 381pp. 71-79.
10. F. H. Dalla Torre, E. V. Pereloma and C. H. J. Davies: *Scr. Mater.*, 2004, vol. 51, pp. 367-371.
11. F. H. Dalla Torre, E. V. Pereloma and C. H. J. Davies: *Acta Mater.*, 2006, vol. 54, pp. 1135-1146.
12. T. Yokoyama: *J. JILM.*, 2001, vol. 51, pp. 544-550.
13. T. Nicholas: *Exp. Mech.*, 1981, vol. 21, pp. 177-185.
14. Japan Institute of Metals and Materials: *Kinzoku Data Book*, 5th ed., Maruzen, Tokyo, 1990, p. 634.
15. H. W. Höppel, J. May, P. Eisenlohr and M. Göken: *Z. Metallkd.*, 2005, vol. 96, pp. 566-571.
16. J. May, H. W. Höppel and M. Göken: *Scr. Mater.*, 2005, vol. 53, pp. 189-194.
17. T. Kunimine, N. Takata, N. Tsuji, T. Fujii, M. Kato and S. Onaka: *Mater. Trans.*, 2009, vol. 50, pp. 64-69.
18. M. Kato, T. Fuji and S. Onaka: *Mater. Trans.*, 2008, vol. 49, pp. 1278-1283.
19. R. Armstrong, I. Codda, R. M. Douthwaite and N. J. Petchac: *Phil. Mag.*, 1962, vol. 7, pp. 45-58.
20. H. Conrad: *High-strength materials*, 1965, John Wiley & Sons, New York.
21. W. Bochniak: *Acta Metall. Mater.*, 1995, vol. 43, pp. 225-233.

22. H. Conrad and D. Yang: *J. Electron Mater.*, 2002, vol. 31, pp. 304–312.
23. H. Conrad: *Mater. Sci. Eng. A*, 2003, vol. 341, pp. 216-228.
24. Y. M. Wang, A. V. Hamza and E. Ma: *Acta Mater.*, 2006, vol. 54, pp. 2715–2726.
25. M. Kato: *Mater. Sci. Eng. A*, 2009, vol. 516, pp. 276-282.
26. T. Kunimine, T. Aragaki, T. Fujii, S. Onaka and M Kato: *J. Mater. Sci.*, 2011, vol. 46, pp. 4302-4307.
27. J. Koike, R. Ohyama, T. Kobayashi, M Suzuki and K. Murayama: *Mater. Trans.*, 2003, vol. 44, pp. 445-451.
28. R. Raj and M. F. Ashby: *Metall. Trans*, 1971, vol. 2, pp. 1113-1127.
29. T. Mori, M. Koda and R. Monzen: *Acta Metall.*, 1983, vol. 31, pp. 275-283.
30. R. Monzen, K. Kitagawa and T. Mori: *Acta Metall.*, 1989, vol. 37, pp. 1619-1625.
31. H. Miura, K. Matsumoto and M. Kobayashi: *J. Jpn. Inst. Met. Mater.*, 2015, vol. 79, pp. 295-302.
32. R. Z. Valiev and O. A. Kaibyshev: *Acta Metall.*, 1983, vol. 31, pp. 2121-2128
33. S. Hwang, C. Nishimura and P. G. McCormick: *Scr. Mater.*, 2001, vol. 44, pp. 1507-1511.
34. A. Ball and M. M. Hutchison: *Metal Sci. Journal*, 1969, vol. 3, pp. 1-7.
35. M. F. Ashby and R. A. Verrall: *Acta Metall.*, 1973, vol. 21, pp. 149-163.
36. R. Monzen and Y. Sumi: *Phil. Mag. A*, 1994, vol. 70, pp. 805-817.

FIGURE and TABLE CAPTIONS

Fig. 1-Bright-field TEM micrograph of an AZ61Mg specimen processed by MDFing of 9 passes ($\Sigma\Delta\varepsilon = 7.2$). The inset is the corresponding selected-area diffraction pattern taken using a selected-area aperture of 2.5 μm in diameter.

Fig. 2-Stress-strain curves of AZ61Mg specimens with different grain sizes produced by MDFing of different passes, tested under strain rates of (a) 10^{-3} and (b) 10^3 s^{-1} at RT.

Fig. 3-Strain rate dependence of the fracture strain of AZ61Mg specimens with different grain sizes fabricated by MDFing. Tensile tests were performed at RT.

Fig. 4-Grain size dependence of the fracture strain of AZ61Mg specimens fabricated by MDFing under a constant strain rate of 10^{-3} s^{-1} at 77 (196 °C), 200 K (-73 °C) and RT.

Fig. 5-Change in the 0.2 pct proof stress with strain rate for AZ61Mg specimens with different grain sizes. Tensile tests were performed at RT.

Fig. 6-Stress-strain curves of AZ61Mg specimens with different grain sizes at (a) 77 K (-196 °C) and (b) RT. The steps on the curves are changes in the flow stress caused by strain-rate jump tests between 10^{-4} and 10^{-3} s^{-1} .

Fig. 7-Relationship between the strain rate sensitivity m and deformation temperature T for AZ61Mg specimens with different grain sizes processed by MDFing.

Fig. 8-AFM images of an AZ61Mg specimen with a grain size of 0.3 μm (a) before and (b) after

tensile deformation of 5 pct plastic strain at RT under a strain-rate of 10^{-5} s^{-1} .

Fig. 9-AFM images and their sectional height profiles of an AZ61Mg specimen with a grain size of $0.3 \mu\text{m}$ (a) before and after tensile deformation of (b) 5 pct and (c) 15 pct plastic strain at RT under a strain-rate of 10^{-5} s^{-1} . All the images were taken from the same area. The arrow indicates the tensile axis.

Fig. 10-Change in the arithmetic average roughness R_{ave} with applied plastic strain under several deformation conditions for an AZ61Mg specimen with a grain size of $0.3\mu\text{m}$.

Fig. 11-Relationship between the normalized activation volume V^* / b^3 and deformation temperature T for AZ61Mg specimens with different grain sizes.

Fig. 12-Bright-field TEM micrograph of an AZ61Mg specimen processed by MDFing of 3 passes ($\Sigma\Delta\varepsilon = 2.4$). The arrows indicate $\beta\text{-Mg}_{17}\text{Al}_{12}$ precipitates.

Table 1-Tensile stress σ_{UTS} , 0.2 pct proof stress $\sigma_{0.2}$ and fracture strain ε_f of AZ61Mg specimens with different grain sizes, obtained under a strain-rate of 10^{-3} s^{-1} . Also shown are the reported data for ZK60-T5 Mg alloy [12] and 6061-T6 Al alloy [13] for the sake of comparison.

Table 2-Fracture strain ε_f , specific strength $\sigma_{\text{UTS}} / \rho$ and absorption energy W of AZ61Mg specimens with different grain sizes, obtained under a dynamic strain-rate condition of 10^3 s^{-1} . Also shown are the reported data for ZK60-T5 Mg alloy [12] and 6061-T651 Al alloy [13] for the sake of comparison.

Table 3-Strain-rate sensitivity m of AZ61Mg specimens with different grain sizes, obtained at RT

from tensile tests under a wide range of strain rates from 10^{-5} to 10^3 s $^{-1}$, and strain-rate jump tests.

TABLES

Table 1

Specimen	σ_{UTS} [MPa]	$\sigma_{0.2}$ [MPa]	ε_f [%]	
AZ61Mg	8 (1 pass)	298	160	36
	2 (3 pass)	350	262	28
	0.5 (6 pass)	363	289	27
	0.3 (9 pass)	390	324	16
ZK60A-T5	328	267	21	
6061-T6	309	278	13	

Table 2

Specimen	ε_f [%]	σ_{UTS} / ρ [Nmg $^{-1}$]	W [Jg $^{-1}$]	
AZ61Mg	8 (1 pass)	22	170	35
	2 (3 pass)	14	191	27
	0.5 (6 pass)	8	219	16
	0.3 (9 pass)	3	261	8
ZK60A-T5	14	219	26	
6061-T6	12	140	15	

Table 3

Specimen	m (tensile test)	m (strain-rate jump test)
8 (1 pass)	0.008	0.004
2 (3 pass)	0.013	0.014
0.5 (6 pass)	0.019	0.023
0.3 (9 pass)	0.023	0.026